Nonlinear dynamics of quantum dot nuclear spins

P. Maletinsky,* C. W. Lai, A. Badolato, and A. Imamoglu
Institute of Quantum Electronics, ETH-Hönggerberg, CH-8093, Zürich, Switzerland
(Dated: February 3, 2008)

We report manifestly nonlinear dependence of quantum dot nuclear spin polarization on applied magnetic fields. Resonant absorption and emission of circularly polarized radiation pumps the resident quantum dot electron spin, which in turn leads to nuclear spin polarization due to hyperfine interaction. We observe that the resulting Overhauser field exhibits hysteresis as a function of the external magnetic field. This hysteresis is a consequence of the feedback of the Overhauser field on the nuclear spin cooling rate. A semi-classical model describing the coupled nuclear and electron spin dynamics successfully explains the observed hysteresis but leaves open questions for the low field behaviour of the nuclear spin polarization.

PACS numbers: 73.21.La, 78.67.Hc, 71.35.Pq, 71.70.Jp, 72.25.Fe, 72.25.Rb

I. INTRODUCTION

Coupling of a single confined electron-spin to a mesoscopic ensemble of nuclear spins defined by a quantum dot (QD) gives rise to rich physical phenomena such as non-Markovian electron-spin decoherence.[1,2,3] It has been argued that controlling QD nuclear spins by carrying out either dynamical nuclear spin polarization (DNSP) or precise measurements of the Overhauser field would prolong the electron spin coherence time and thereby enhance the prospects of implementing QD spin-based quantum information processing.[4] Several groups have previously reported QD nuclear-spin cooling in various QD systems.[5,6]A non-trivial dependence of DNSP on the applied external magnetic field however, was never observed at high fields. Recently, DNSP in self-assembled InGaAs QDs was reported for low external magnetic fields.[7,8] Experiments carried out using resonant excitation of the QD excited-states showed that DNSP can be observed even when the external field vanishes: this has been attributed to the role of the inhomogeneous electronic Knight field in suppressing depolarization due to the spin-non-conserving part of the nuclear dipole-dipole interactions. An obvious extension of this work is to study the limits on the degree of DNSP that can be attained in these QDs by, for example, investigating the external magnetic field dependence.

In this work, we study the magnetic field dependence of DNSP in a single self-assembled QD. The QD is located in a gated structure that allows for deterministic QD charging with a single excess electron[9] or hole.[10] The photoluminescence (PL) polarization and spin splitting are studied by resonantly exciting the QD in one of its (discrete) excited (p-shell) states under external magnetic fields (B_{ext}) ranging from $B_{\text{ext}} = -2$ to 2 T, applied along the crystal growth z-axis at $T = 2.5$ K. The PL spectral lines associated with different charging states of a single QD can be identified from a PL intensity contour plot as a function of the bias voltage and emission energy.[9] In this work, we focus on the spectral features of the negatively charged exciton (X^{-1}), consisting of two electrons in a spin singlet state and one hole trapped in the QD. This charge complex has been shown to lead to a polarization of the underlying nuclear spin system under circularly polarized excitation.[8]

The sample was grown by molecular beam epitaxy on a (100) semi-insulating GaAs substrate. The InAs QDs are spaced by 25 nm of GaAs from a 40 nm doped n^{++}-GaAs layer, followed by 30 nm GaAs and 29 periods of AlAs/GaAs (2/2 nm) superlattice barrier layer, and capped by 4-nm GaAs. A bias voltage is applied between the top Schottky and back ohmic contacts to control the charging state of the QDs. The low density of QDs ($< 0.1\,\mu\text{m}^{-2}$) allows us to address a single QD using a micro-photoluminescence (μ-PL) setup.

Our standard μ-PL setup[8] is based on the combination of a solid immersion lens, directly fixed onto the sample, and a focussing lens mounted outside the cryostat. The sample is placed in a Helium-bath cryostat equipped with a superconducting magnet, reaching a maximum magnetic field strength of 10 T and oriented in the Faraday geometry. The spectroscopy system consists of a spectrometer of 0.75 m focal length and a liquid-nitrogen cooled CCD camera providing a spectral resolution of ~ 20 μeV. The energies of the QD PL lines are determined by estimating the center of mass of the observed emission lines by calculating a weighted average over the relevant CCD pixels. We estimate the resulting accuracy in our energy measurement to be ~ 2 μeV.

We have performed measurements on the negatively charged exciton X^{-1} at the center of its PL stability region with respect to gate voltage. In this regime, electron co-tunnelling to the nearby reservoir has shown to be minimized[11] and the QD is occupied with a single electron in its ground state. Optical excitation is performed in a resonant way into the p-shell, which lies approximately one LO phonon energy above the emission energy of X^{-1} ($E_0 = 1.316524$ eV). The excitation power is fixed close to saturation of the observed emission line. We found that these conditions lead to a maximal preservation of PL light polarization ($\sim 75\%$ at $B = 0$ T) after excitation with circularly polarized light.

For X^{-1}, circular polarization of the emitted light reflects both the spin of the hole in the QD state before

emission and the initial spin of the residual electron in the QD after photon emission. A high degree of circular polarization of X^{-1}-emission thus indicates a highly spin polarized residual electron in the QD. Since the electron spin system is in thermal contact with the nuclear spin system through the hyperfine interaction, spin polarization (or temperature) will be transferred from one to the other, thereby cooling the nuclear spin system. At the same time, nuclear spin diffusion, quadrupolar interactions and other nuclear spin relaxation mechanisms will heat up the nuclear spin system, leading to its finite spin temperature in a dynamical equilibrium. In the following, we want to study these spin-transfer mechanisms and the dependence of the final nuclear spin temperature on an external magnetic field $B_{\rm ext}$ along the spin quantization axis.

II. HYPERFINE INTERACTION

The dominant contribution to the coupling between the electron- and the nuclear-spin systems originates from the Fermi contact hyperfine interaction. For an electron in a QD and in first order perturbation theory, this can be written as[12]

$$\hat{H}_{\rm hf} = \frac{\nu_0}{8}\sum_i A_i|\psi(\mathbf{R}_i)|^2\hat{\mathbf{S}}\cdot\hat{\mathbf{I}}^i, \qquad (1)$$

where ν_0 is the volume of the InAs-crystal unit cell containing eight nuclei, $\hat{\mathbf{S}}$ is the dimensionless electron spin operator, $\psi(\mathbf{r})$ is the electron envelope wave function and $\hat{\mathbf{I}}^i$ and $\mathbf{R}_i$ are the spin and location of the i-th nucleus, respectively. $A_i = (2\mu_0 g_0\mu_{\rm B}\mu_i/3I^i)|u(\mathbf{R}_i)|^2$ is the hyperfine coupling constant, which depends on the nuclear magnetic moment μ_i, the nuclear spin I^i and on the value of the electron Bloch function $u(\mathbf{R}_i)$ at the nuclear site. $\mu_{\rm B}$ is the Bohr magneton, g_0 the free electron g-factor and μ_0 the permeability of free space. A_i is positive and is on the order of 50 μeV for all the nuclei in our system.

With the identity $\hat{\mathbf{S}}\cdot\hat{\mathbf{I}}^i = 1/2(I^i_+S_- + I^i_-S_+) + I^i_zS_z$ where $I^i_\pm$ and $S_\pm$ are the nuclear and electron spin raising and lowering operators respectively, equation (1) can be decomposed into two parts:[13] A dynamical part ($\propto I^i_+S_- + I^i_-S_+$), allowing for the transfer of angular momentum between the two spin systems and a static part ($\propto I^i_zS_z$), affecting the energies of the two spin systems. In the absence of any other relaxation mechanisms, the dynamical contribution leads to an equilibrium mean nuclear spin polarization $\langle I^i_z\rangle$ along the quantization axis z, given by[14]

$$\langle I^i_z\rangle = \frac{I^i(I^i+1)}{S(S+1)}\langle S_z\rangle, \qquad (2)$$

where $\langle S_z\rangle$ is the mean electronic spin along the z-axis. This equation is valid if $\langle I^i_z\rangle \ll I^i$ and if we neglect any polarization due to thermalization in an external magnetic field of either of the two spin systems.

The static part leads to the notion of the "effective magnetic field", either seen by the electron due to spin polarized nuclei (Overhauser field), or by the nuclei due to a spin polarized electron (Knight field). The effects of the Knight field on the order of $10-100$ G upon the nuclear spin system have been studied elsewhere[8] and will not be considered in the present work. The Overhauser field operator can be written as

$$\hat{B}_{\rm nuc} = \frac{1}{g^*_{\rm el}\mu_{\rm B}}\frac{\nu_0}{8}\sum_i A_i|\psi(\mathbf{R}_i)|^2\hat{I}^i_z, \qquad (3)$$

and has a finite expectation value $B_{\rm nuc}$ if the nuclei are partly polarized. This effective field leads to a total electron Zeeman splitting in the presence of both, nuclear and external magnetic fields of

$$\Delta E^Z_{\rm el} = g^*_{\rm el}\mu_{\rm B}(B_{\rm ext}+B_{\rm nuc}). \qquad (4)$$

The energy shift due to spin polarized nuclei is referred to as Overhauser shift (OS). We note that only electrons in the conduction band experience a substantial OS. For carriers in the valence band, the contact hyperfine interaction (1) vanishes due to the p-type symmetry of this band in *III-V* semiconductors. Since the electrons in X^{-1} are in a singlet state, they are not affected by $B_{\rm nuc}$ either and only the final state of recombination shifts due to nuclear polarization. The total Zeeman splitting of the X^{-1} recombination line thus amounts to

$$\Delta E^{\rm Z}_{X^{-1}} = -g^*_{\rm h}\mu_{\rm B}B_{\rm ext} - g^*_{\rm el}\mu_{\rm B}(B_{\rm ext}+B_{\rm nuc}), \qquad (5)$$

where $g^*_{\rm el}$ and g^*_h are the electron- and hole g-factors, respectively.

Exciting the QD with linearly polarized light creates residual electrons in a superposition of spin up and down, resulting in no nuclear polarization and $B_{\rm nuc} = 0$ T. Thus, comparing the Zeeman splittings of X^{-1} under linearly- and circularly polarized excitation ($\Delta E^{\rm Z,lin.}_{X^{-1}}$ and $\Delta E^{{\rm Z},\sigma^\pm}_{X^{-1}}$, respectively) gives a direct measure of $B_{\rm nuc}$:

$$\Delta E^{{\rm Z},\sigma^\pm}_{X^{-1}} - \Delta E^{\rm Z,lin.}_{X^{-1}} = -g^*_{\rm el}\mu_{\rm B}B_{\rm nuc}. \qquad (6)$$

III. EXPERIMENTAL PROCEDURE

In order to gain knowledge about the nuclear polarization and its dependence on an external magnetic field along the spin quantization axis in QDs, we performed a μ-PL experiment on a single QD in an external magnetic field with the experimental procedure proposed above. Nuclear polarization manifests itself in a difference in emission energies between excitation with circularly and linearly polarized light as was established in the previous section. Figure 1 shows the X^{-1}-emission energies of a single QD under excitation with circularly polarized light as a function of external magnetic field. Throughout this paper, red (black) color denotes excitation with σ^+ (σ^-) light, while squares (triangles) stand for co- (cross-)

circular detection. The polarizations for excitation and detection are denoted as $(\sigma^\alpha, \sigma^\beta)$ where σ^α and σ^β correspond to excitation and detection, respectively. The index α or β ($\alpha, \beta \in [+, -]$) stands for circularly polarized light with positive or negative helicity. The data shown in figure 1 was obtained in a single sweep from $B = -2$ T to $B = +2$ T, varying excitation and detection polarization for each B-field value in the order $(\sigma^+, \sigma^-) \Rightarrow (\sigma^+, \sigma^+) \Rightarrow (\sigma^-, \sigma^+) \Rightarrow (\sigma^-, \sigma^-)$ such that any memory of the nuclear spin system is erased during the sweep. The data for $|B| < 500$ mT was taken with smaller magnetic field steps in order to highlight the detailed behavior of DNSP at low fields. Every data point represents the center of mass of the emission peak of X^{-1} taken from a single spectrum with 1 s integration time and a signal to noise ratio of $\sim 100:1$ for co-circular detection. The effects of nuclear polarization can be seen in the range of $|B_{\text{ext}}| < 1.2$ T where emission energies for a given detection polarization depend strongly on the helicity of the laser light. Excitation with σ^+ light creates a residual electron with its spin pointing in the positive z-direction (see Fig.1). According to equations (1) and (3), this creates a nuclear spin polarization in the same direction and, due to the negative sign of the g^*_{el}, a nuclear field pointing in the negative z-direction. This scenario is consistent with the polarization sequences and lineshifts observed in Fig. 1. Above 1.2 T, the emission energies of the QD are almost independent of excitation light polarization, indicating that nuclear effects become very small. Another striking feature in this data is the symmetry under simultaneous reversal of the excitation light helicity and the sign of the magnetic field. However, the data is not symmetric under the reversal of only one of these parameters. This asymmetry indicates that the system distinguishes between nuclear fields pointing along or against the external magnetic field - we will see in the following that it is more efficient for the system to create a nuclear field pointing against B_{ext} than one that points along this field.

In order to obtain a more quantitative picture of the magnetic field dependent DNSP, we performed the following analysis steps on the data (see Fig. 2): We first extract the Zeeman splittings for excitation with σ^+ and σ^- light from the raw data shown in Fig. 1. To this data, we fit a linear Zeeman splitting such that the fit coincides with the data at magnetic fields $B_{\text{ext}} > 1.8$ T where nuclear polarization is very small (Fig. 2(a)). The excitonic g-factor, $g_{\text{ex}} = 1.87$[18], that we find with this fitting procedure matches within a few percent to an independent measurement of g_{ex} that we performed with linearly polarized excitation (not shown here). The Overhauser shift can now be extracted from this fit with the help of equation (6); the result is plotted in figure 2(b). There's a striking difference when polarizing the nuclei along or against the external field: Nuclear polarization with B_{nuc} pointing along the applied field is rather inefficient and shows a slight decrease with increasing magnitude of the applied field. Polarization with B_{nuc} pointing against the external magnetic field on the other hand shows a much richer behavior: The nuclear polarization first increases almost linearly as the magnitude of the external field increases and then shows a sudden drop when $|B| > 1.2$ T.

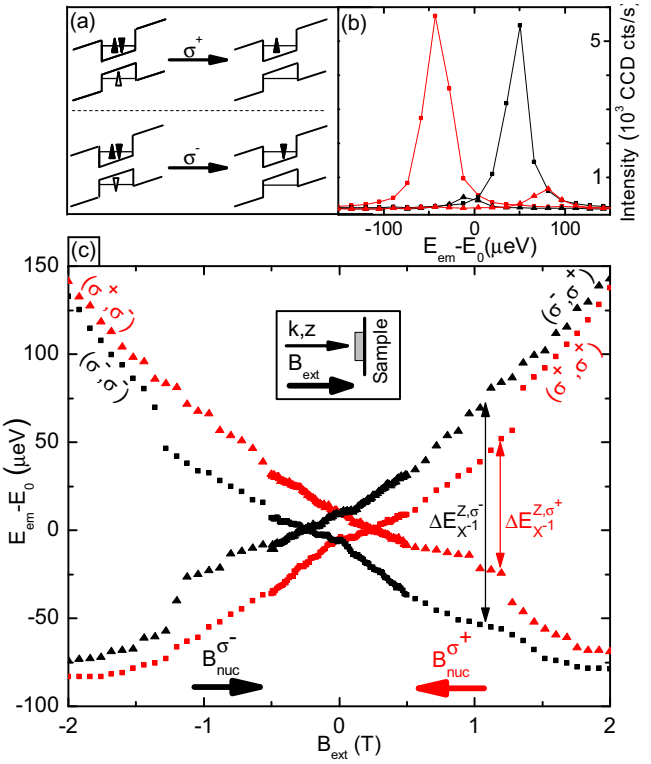

FIG. 1: (color online). **(a)** Spin configurations of X^{-1} before and after the emission of a $\sigma^\pm$ polarized photon. Open (filled) triangles denote the spin of the hole (electron). **(b)** Raw spectra at $B_{\text{ext}} = -0.96$ T for the four excitation/detection configurations in the circular basis: red (black) denotes excitation with σ^+ (σ^-) polarized light. Detection is co- or cross-circular (squares and triangles, respectively). **(c) Energy dispersion of X^{-1} under circularly polarized excitation:** The different emission energies (E_{em}) for the two excitation polarizations are due to dynamical nuclear spin polarization which leads to an effective nuclear magnetic field $B^{\sigma\pm}_{\text{nuc}}$ under $\sigma^\pm$ excitation (orientation indicated by the arrows in the figure). The energy $E_0 = 1.316524$ eV of the X^{-1} emission under linearly polarized excitation at $B = 0$ T is subtracted from the data. The inset shows the relative orientation of k-vector, quantization axis z and positive magnetic field.

From the spectral data we can also extract information about the hole spin polarization before- and the residual electron spin polarization after recombination of X^{-1}. For this, we define a degree of QD spin polarization as $\rho_c^\pm := (I_{(\sigma^\pm,\sigma^+)} - I_{(\sigma^\pm,\sigma^-)})/(I_{(\sigma^\pm,\sigma^+)} + I_{(\sigma^\pm,\sigma^-)})$ under $\sigma^\pm$ excitation. $I_{(\sigma^\alpha,\sigma^\beta)}$ are the intensities of the dominant PL-peaks in the corresponding analyzer/polarizer configurations ($\alpha, \beta \in [+, -]$). We note that at zero magnetic field, $\rho_c^\pm$ is identical to the degree of circular polarization of the single PL peak observed. The measured quantity $\rho_c^\pm$ is plotted in figure 2(c) as a function of external magnetic field. It is roughly constant and on the order of 85%

over a wide range of magnetic fields. Only for the fields where the trion Zeeman splitting vanishes, $\rho_c^{\pm}$ shows a dip to roughly 65%. This behavior is consistent with the rotation of the exciton spin during relaxation of the optically created electron from the excited p-shell state to the s-shell via the electron reservoir.[8] During the relaxation, the QD is left neutral and anisotropic exchange interaction will rotate the exciton spin. This rotation is most efficient in the absence of excitonic Zeeman splitting which explains the magnetic field dependence of PL polarization observed in this measurement.

We note however that there is a certain asymmetry in the data shown in figure 2(c) that remains unexplained: ρ_c^- is larger than ρ_c^+ at high magnetic fields and the dip in ρ_c^- at lower fields is less pronounced than for ρ_c^+. A possible reason for this asymmetry could be the different excitation efficiencies in the QD for σ^+ and σ^- excitation.

IV. MODELLING OF THE DATA

Most of the above-mentioned nuclear effects in the presence of an external magnetic field can be described by a simple rate equation model already proposed earlier[7,15] and originally based on the work by Abragam.[14] The rate equation is based on the condition for thermal equilibrium (2) between the electron and the nuclear spin system in the absence of any coupling to the environment. This equilibrium is then reached on a typical timescale given by the nuclear spin relaxation time T_{1e}, which can be estimated to be[13]

$$\frac{1}{T_{1e}} = \frac{1}{T_{1e}^0}\frac{1}{1+\Omega_{el}^2\tau_{el}^2}. \qquad (7)$$

Here, τ_{el} is the electron spin correlation time which broadens the electronic spin states. $\Omega_{el} = \Delta E_{el}^Z/\hbar$ is the electron Larmor frequency. This frequency itself depends on the degree of nuclear polarization through (4) and (3). For a given nuclear species, the nuclear spin relaxation time at zero electron Zeeman splitting is given by $1/T_{1e}^0 = f_{el}\tau_{el}A_i^2/(N\hbar)^2$ with N the number of relevant nuclei and f_{el} the fraction of time the QD is occupied with a single electron. This expression for T_{1e}^0 is valid if we assume a homogenous electron wave function $\psi(\mathbf{r}) \propto \sqrt{8/\nu_0 N}$ which is constant within the QD volume and zero outside.

By adding a nuclear spin decay channel which is dominated by nuclear spin diffusion out of the QD on a timescale T_d, we end up with a rate equation of the form

$$\frac{d\langle I_z^i\rangle}{dt} = -\frac{1}{T_{1e}}(\langle I_z^i\rangle - \frac{4}{3}I^i(I^i+1)\langle S_z\rangle) - \frac{1}{T_d}\langle I_z^i\rangle. \qquad (8)$$

This equation was obtained for the coupling of a single electron to a single nuclear spin. It can be approximately generalized to the case of an ensemble of different nuclei in the QD by considering the mean nuclear spin polarization $\langle I_z\rangle = \frac{1}{N}\sum_i\langle I_z^i\rangle$. For this, we replace the hyperfine

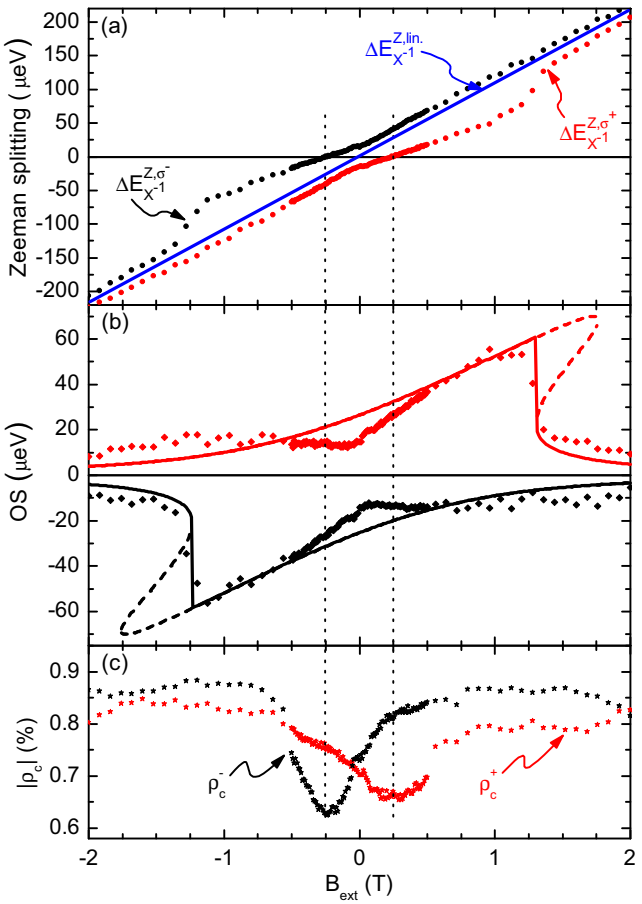

FIG. 2: (color online). **Nuclear Polarization in external magnetic fields: (a)** Spin splitting of X^{-1} under circularly polarized excitation (Circles). Red represents σ^+, black σ^- excitation. The solid line is a linear fit to the data as described in the text. **(b)** Deviation of spin splitting between circular and linear excitation: Overhauser shift for σ^+ and σ^- excitation (red and black diamonds, respectively). The solid and dashed lines are the results of the fits according to the model discussed in the text. **(c)** QD spin polarization $\rho_c^{\pm}$ of PL light under $\sigma^{\pm}$ excitation. The polarization shows a minimum at the magnetic field where the Zeeman splitting is zero, consistent with our model of carrier relaxation.[8]

constant A_i in (7) and the quantity $I^i(I^i+1)$ in (8) each by a weighted average $\overline{\zeta} = 0.5(x\zeta_{In} + (x-1)\zeta_{Ga} + \zeta_{As})$. x and $(1-x)$ are the relative contents of In and Ga in the QD (a typical value for our QDs is $x = 0.9$) and ζ represents the variable to be averaged over the different nuclear species (A_i or $I^i(I^i+1)$). With values of A_i taken from the literature[16], this results in $\overline{A^i} = 50.3$ μeV and $\overline{I^i(I^i+1)} = 13.2$. We take these numbers to be fixed in the following, even though in reality they might vary due to uncertainties in QD composition and confined electron wave-function.

Since the electron-mediated nuclear spin relaxation time T_{1e} itself depends on nuclear spin polarization, equation (8) leads to the following self-consistent nonlinear

steady state solution $\langle I_z^{\rm ss}\rangle$ for the mean nuclear spin polarization:

$$\langle I_z^{\rm ss}\rangle = \frac{4}{3}\frac{\overline{I^i(I^i+1)}\langle S_z\rangle}{1+\frac{T_{1e}^0}{T_d}(1+(\frac{\tau_{el}}{\hbar})^2(g_{el}^*\mu_B B+\overline{A_i}\langle I_z^{\rm ss}\rangle)^2)}. \quad (9)$$

For the fitting procedure we take $\langle S_z\rangle$ to be independent of magnetic field and equal to half the mean PL polarization $\rho_c^{\pm}/2$ observed in the experiment for $|B_{\rm ext}| > 0.5$ T. We note that using the magnetic field dependent $\rho_c^{\pm}$ measured in the experiment (Fig. 2(c)) did not lead to a significant improvement of the fits and is thus not shown here. It also has to be noted that the way we averaged equation (9) over the different nuclear species as well as the fact that we used a homogenous wavefunction for the electron and that we neglected the magnetic field dependence of T_d all limit the validity of this model.

We numerically solved the implicit equation (9) in order to fit the data. The result of such a numerical solution is shown in figure 2(b). The model qualitatively reproduces the data. Still, some features, like the fast change of DNSP around zero external field as well as the high residual spin polarization at high external magnetic fields, could not be explained within the model. In the region 1.2 T$< B_{\rm ext} <$ 1.8 T the model predicts three solutions: two stable states, one with a low and one with a high degree of DNSP and an unstable solution of intermediate nuclear spin polarization (the last two solutions correspond to the dashed lines in Fig. 2). Since in this experiment we changed excitation polarization from σ^+ to σ^- for each magnetic field value, the system always followed the solution with minimal nuclear spin polarization and DNSP dropped at $B_{\rm ext} \simeq 1.2$ T. The fact that the drop in DNSP in this measurement was rather smooth compared to the model prediction was probably due to the very long timescale of the buildup of DNSP right before its disappearance: since in the experiment every point was taken with an integration time of 1 s, the nuclear system did not have time to reach its steady state polarization before the excitation light polarization was switched. We will discuss this breakdown of DNSP as well as the regime of high nuclear spin polarization and bistability in more detail in the following section. The parameters used for the fitting curve in figure 2(b) were $T_{1e}^0/T_d = 4.3$,$\rho_c = 0.84$,$\tau_{el} = 35$ ps, $g_{el}^* = -0.69$, which are all realistic values for our QD. The electron spin correlation time found in the fit can be explained in a simple three level picture where the QD is excited from its ground state into its p-shell and PL emission is observed from carriers recombining from the s-shell. Since this system is pumped close to saturation, the lifetime and thus the coherence time of the residual electron are limited by the relaxation time from the p-shell to the n^{++}-GaAs layer by tunnelling. This timescale is expected to be shorter than 20 ps.[8]

The parameters obtained in this fit also allow us to estimate the nuclear spin relaxation time T_{1e}^0. Using the value $\tau_{el} = 35$ ps, the corresponding value for $f_{el} = 0.035$ (assuming an exciton lifetime of 1 ns) and N$= 10^4 - 10^5$, we obtain $T_{1e}^0 = 0.1-1$ s. This value is roughly consistent with the buildup time of nuclear spin polarization we observed.[8]

We extended the presented model by including the dynamics of the mean electron spin $\langle S_z\rangle$. This leads to a rate equation for the electron spin of a form similar to equation (8). The main differences between the electron and the nuclear spin dynamics are that the electron spin system in the absence of losses reaches the thermal equilibrium state (2) at a rate N/T_{1e}. Compared to the nuclear spin relaxation rate, the electron spin relaxation is faster by the number of nuclei N in the system. In addition, the electron spin is repumped into its initial state $S_z^0 = \rho_c^{\pm}/2$ at the s-shell decay rate on the order of 1 ns. This extension however, did not lead to any new insights on the behavior of the nuclear spin system. A numerical study of this extended model suggested though that the mean electron spin decreases linearly with increasing nuclear spin polarization. The electron spin thus seems to follow the intricate dynamics of the nuclear spin system. This observation motivates further studies on the positively charged exciton where PL light polarization gives a direct measure of the mean electron spin.

V. HYSTERESIS IN THE MAGNETIC FIELD SWEEPS

In this section, we focus on the bistable behavior of the coupled electron-nuclear spin system in the magnetic field range close to the "breakdown" of DNSP. Figure 3 shows a graphical representation of the solutions of the nonlinear equation (9). The result suggests that the maximal achievable degree of DNSP in our system leads to a maximal OS given by $\mathrm{OS}_{\rm max} = \frac{4}{3}\overline{A_i}\,\overline{I^i(I^i+1)}\langle S_z\rangle(1+T_{1e}^0/T_d)^{-1}$. this value is reached when nuclear spin relaxation is maximized, i.e. when the total electron Zeeman splitting is zero (cf. equation (9)). It can also be seen from the figure that there is a regime of external magnetic fields where two stable solutions for DNSP coexist. One solution leads to a high degree of nuclear polarization, reaching $\mathrm{OS}_{\rm max}$ at its maximum, while the other one shows a low degree of nuclear polarization. The graphical solution also shows that bistability is an inherent property of the solutions of equation (8) for systems where $\mathrm{OS}_{\rm max}$ is at least on the order of the width of the electronic spin states ($\hbar/\tau_{el}$), which is typically the case for localized carriers such as in QDs, but not for bulk systems. The two stable solutions can be understood as follows: When increasing an external field while creating a nuclear field in the opposite direction, the electron Zeeman splitting is reduced compared to the case of no nuclear polarization. This keeps nuclear spin relaxation at a high rate T_{1e}^{-1} such that DNSP can be maintained. As soon as $\mathrm{OS}_{\rm max}$ is reached, however, the system can no further compensate for an increasing external magnetic field. DNSP will start to drop, which eventually leads to

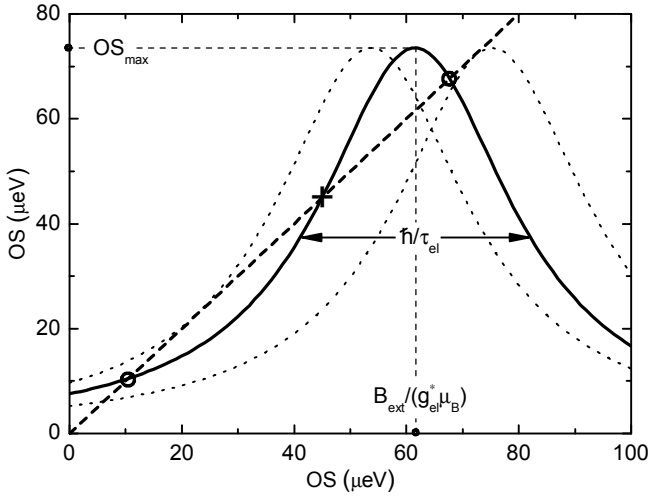

FIG. 3: **Graphical solution of equation (9):** solid (dashed) line: right (left) hand side of equation (9). These terms correspond to gain and loss of DNSP, respectively. Circles (cross) indicate the stable (unstable) solutions for nuclear spin polarization. The center of the Lorentzian shifts proportionally to the external magnetic field, explaining the magnetic field dependence of DNSP. The two dotted curves show the situation at the critical fields B_1 and B_2. It can be seen directly from the figure that: 1.) Bistability can only be observed if the slope of the Lorentzian at its half width is bigger than 1 and 2.) the difference between the two critical external fields where either one of the stable solutions vanishes is on the order of the width of electron spin states in units of magnetic fields $\hbar/(\tau_{\rm el} g^*_{\rm el}\mu_{\rm B})$.

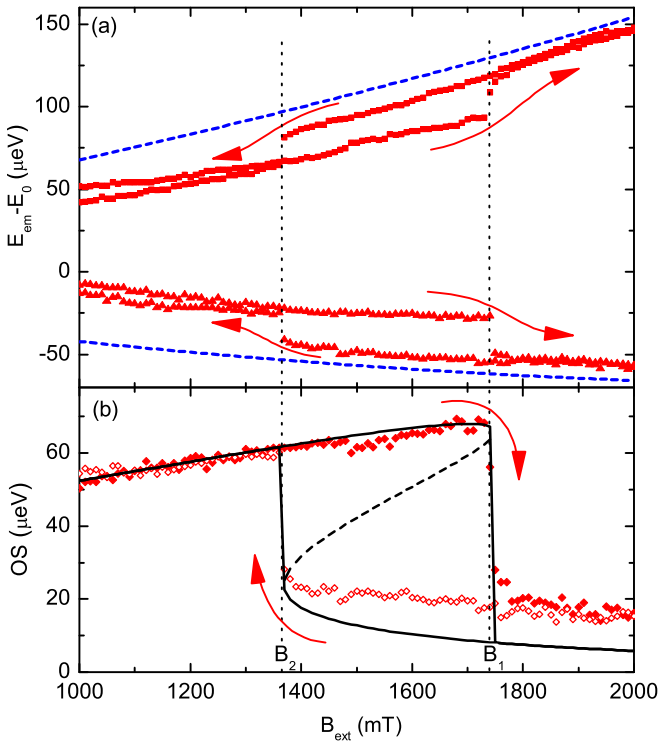

FIG. 4: (color online). **Hysteresis behavior of the coupled electron-nuclear spin-system:** Magnetic field sweeps under excitation with constant light polarization (σ^+). **(a)** X^{-1} emission energies, sweeping magnetic field up or down (indicated by arrows). Squares (triangles) denote co- (cross-) circular detection with respect to excitation polarization. The dashed line is a fit to the case of linearly polarized excitation. **(b)** Overhauser shifts extracted from the data shown in (a) for the magnetic field sweeping up and down (solid and open diamonds, respectively). The black line shows the simulations described in the text.

an abrupt jump of DNSP to a low value at an external field B_1. This jump is due to the negative feedback of the low DNSP on T_{1e}^{-1}. When ramping the external field down again, now in the absence of nuclear polarization, the system will initially remain in a state of low DNSP since T_{1e}^{-1} is still low. DNSP will slightly increase though due to the increasing rate T_{1e}^{-1} of nuclear polarization with decreasing magnetic field strength. At a field B_2, the positive feedback of increasing DNSP on T_{1e}^{-1} will take over and an abrupt jump to a state of high nuclear polarization will occur. As can be seen from figure 3, the difference between the fields B_1 and B_2 is on the order of the width of the electronic spin states in units of magnetic fields.

A hint for bistability in the present system can already be seen in the fit shown in figure 2(b). In order to observe the hysteretic behavior of the system we performed a magnetic field dependent PL experiment as described above, now by exciting the QD with light of constant helicity and by ramping the magnetic field from low to high and back again. Hysteretic behavior can be expected if the nuclear fields created in that way are pointing against the external magnetic field. In our system such a situation is realized when exciting the QD with σ^+ light and applying an external field in the positive z-direction.

Figure 4 shows data obtained in this regime: Going from low to high field amplitude, DNSP is significant up to a magnetic field value of $B_1 = 1.74$ T where it suddenly drops. Sweeping the magnetic field back to low field amplitudes DNSP reappears at a field $B_2 = 1.36$ T, a value different from B_1. The difference of 380 mT between these two field is on the order of $\hbar/(\tau_{\rm el} g^*_{\rm el}\mu_{\rm B})$ as predicted by the model.

Also shown in figure 4 is a fit of equation (2) to the data. The parameters used for this fit were $T_{1e}^0/T_{\rm d} = 4.54$, $\rho_c = 0.84$, $\tau_{\rm el} = 32$ ps, $g^*_{\rm el} = -0.68$, which are consistent with the parameters used in the fit shown in figure 2. As in the previous fit, the reminiscent nuclear polarization at high fields observed in the experiment is slightly higher than what is predicted by the model.

VI. CONCLUSION

To summarize, we presented a study of the magnetic field dependence of DNSP in a single resonantly pumped

QD. We show clear evidence of the nonlinear behavior of the tightly coupled electron and nuclear spin system and show hysteresis as one example of (spin-)memory of the nuclear spins. A simple rate equation model is used to reproduce and fit our experimental findings. From the model and the experimental data we deduce that a spin polarized electron in an external field can create a nuclear field that actually overcompensates the applied field: in this situation, the electrons and holes in the QD feel effective magnetic fields pointing in opposite directions. Increasing the external field leads to higher nuclear fields, until a maximal achievable nuclear polarization is reached at $B_{\rm ext} = B_1 = 1.74$ T. At that point, the total effective magnetic field acting on the electron is zero. This point is of particular interest because it enables a direct measure of the maximal nuclear field which we find to be $B_{\rm nuc} = 1.74$ T and of the hole g-factor $g_h^* = -1.2$.

The experiment along with the model also shows that the maximal nuclear polarization of $\sim 18\%$ achieved in our system is limited by the fraction $T_{\rm d}/T_{\rm 1e}^0$, i.e. the ratio between nuclear spin decay time and electron mediated nuclear spin relaxation time. While $T_{\rm d}$ is a fixed parameter given by the nature of the QD, $T_{\rm 1e}^0$ could potentially be modified by varying the pump power or the details of the excitation process.[17]

An extension of the model which includes the dynamics of the electron spin shows that this spin is linked to the nuclear spins through a linear relationship. This suggests that not only nuclear spins but also the electron spin shows a bistable behavior at certain experimental conditions. This speculation could be further tested in an experiment on the positively charged exciton where PL light polarization directly probes the mean electron spin.

The qualitative disagreement of the model with our data in the low field range where the measured DNSP shows a clear "kink" as a function of magnetic field, indicates that our simple approach does not give a full description of the nonlinear processes that lead to an equilibrium state of spins in a QD. A further extension of the model could include quadrupolar couplings of the nuclei which would most effectively depolarize the nuclei at low external fields. While our rate equation approach was purely classical, it could also be conceived that the quantum mechanical nature of the electron spin system would alter the behavior of DNSP at low fields and explain the unpredicted features in our measurement. To confirm this hypothesis further theoretical studies would be required.

Acknowledgments

We would like to acknowledge O. Krebs for fruitful discussions about the modelling and helpful inputs about the hysteresis measurements. Further, we would like to thank V.I. Fal'ko, G.Burkhard, S.D. Huber and A. Högele for interesting discussions and help with the manuscript and J. Dreiser for assistance with sample preparation. This work is supported by NCCR-Nanoscience.

* patrickm@phys.ethz.ch

1. A. V. Khaetskii, D. Loss, and L. Glazman, Phys. Rev. Lett. **88**, 186802 (2002).
2. A. C. Johnson, J. R. Petta, J. M. Taylor, A. Yacoby, M. D. Lukin, C. M. Marcus, M. P. Hanson, and A. C. Gossard, Nature **435**, 925 (2005).
3. F. H. L. Koppens, J. A. Folk, J. M. Elzerman, R. Hanson, L. H. W. van Beveren, I. T. Vink, H. P. Tranitz, W. Wegscheider, L. P. Kouwenhoven, and L. M. K. Vandersypen, Science **309**, 1346 (2005).
4. W. A. Coish and D. Loss, Phys. Rev. B **70**, 195340 (2004).
5. D. Gammon, S. W. Brown, E. S. Snow, T. A. Kennedy, D. S. Katzer, and D. Park, Science **277**, 85 (1997).
6. K. Ono and S. Tarucha, Phys. Rev. Lett. **92**, 256803 (2004).
7. B. Eble, O. Krebs, A. Lemaitre, K. Kowalik, A. Kudelski, P. Voisin, B. Urbaszek, X. Marie, and T. Amand (2005), cond-mat/0508281.
8. C. Lai, P. Maletinsky, A. Badolato, and A. Imamoglu, Phys. Rev. Lett. **96**, 167403 (2006).
9. R. J. Warburton, C. Schaflein, D. Haft, F. Bickel, A. Lorke, K. Karrai, J. M. Garcia, W. Schoenfeld, and P. M. Petroff, Nature **405**, 926 (2000).
10. M. Ediger, P. A. Dalgarno, J. M. Smith, B. D. Gerardot, R. J. Warburton, K. Karrai, and P. M. Petroff, Applied Physics Letters **86**, 211909 (2005).
11. M. Atatüre, J. Dreiser, A. Badolato, A. Högele, K. Karrai, and A. Imamoglu, Science **312**, 551 (2006).
12. I. A. Merkulov, A. L. Efros, and M. Rosen, Phys. Rev. B **65**, 205309 (2002).
13. F. Meier, *Optical orientation* (North-Holland, Amsterdam, 1984).
14. A. Abragam, *The principles of nuclear magnetism* (Clarendon Press, Oxford, 1961).
15. D. Gammon, A. L. Efros, T. A. Kennedy, M. Rosen, D. S. Katzer, D. Park, S. W. Brown, V. L. Korenev, and I. A. Merkulov, Phys. Rev. Lett. **86**, 5176 (2001).
16. R. Weast, *Handbook of chemistry and Physics* (The chemical Rubber Co, Ohio, 1968).
17. P.-F. Braun, B. Urbaszek, T. Amand, X. Marie, O. Krebs, B. Eble, A. Lemaitre, and P. Voisin (2006), cond-mat/0607728.
18. We use the following sign convention of Zeeman Hamiltonians for electrons, holes and excitons, respectively: $H_{\rm el} = \mu_B g_{\rm el}^* \mathbf{S}_{\rm el} \cdot \mathbf{B}$, $H_{\rm h} = -\mu_B g_{\rm h}^* \mathbf{S}_{\rm h} \cdot \mathbf{B}$, $H_{\rm ex} = \frac{1}{2}\mu_B g_{\rm ex} \mathbf{S}_{\rm ex} \cdot \mathbf{B}$. In this representation, the heavy-hole wave functions $|\pm\frac{3}{2}\rangle$ convert to pseudo-spins $|\pm\frac{1}{2}\rangle$. With this convention, the exciton g-factor amounts to $g_{\rm ex} = -g_{\rm el}^* - g_{\rm h}^*$. Experimentally, we then find $g_{\rm el}$ and $g_{\rm h}$ to be < 0.